Pilot-scale outdoor photobioreactor culture of the marine dinoflagellate *Karlodinium veneficum*: Production of a karlotoxins-rich extract

L. López-Rosales[a], A. Sánchez-Mirón[a,*], F. García-Camacho[a], A. R. Place[b], Yusuf Chisti [c], E. Molina-Grima[a]

[a] Chemical Engineering Area, University of Almería, 04120 Almería, Spain

[b] Institute of Marine & Environmental Technology, University of Maryland Center for Environmental Science, 701 E. Pratt Street, Baltimore, MD 21202, USA

[c] School of Engineering, Massey University, Palmerston North, New Zealand

*Address correspondence to:
A. Sánchez-Mirón, Chemical Engineering Area, University of Almería, 04120 Almería, Spain
E-mail: asmiron@ual.es; phone: 34-950214025; fax: 34-950015491

Graphical Abstract (for review)

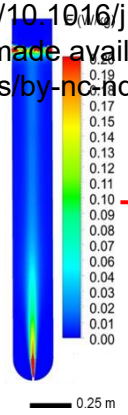

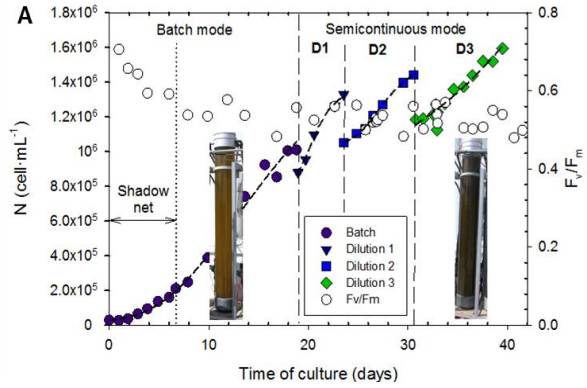

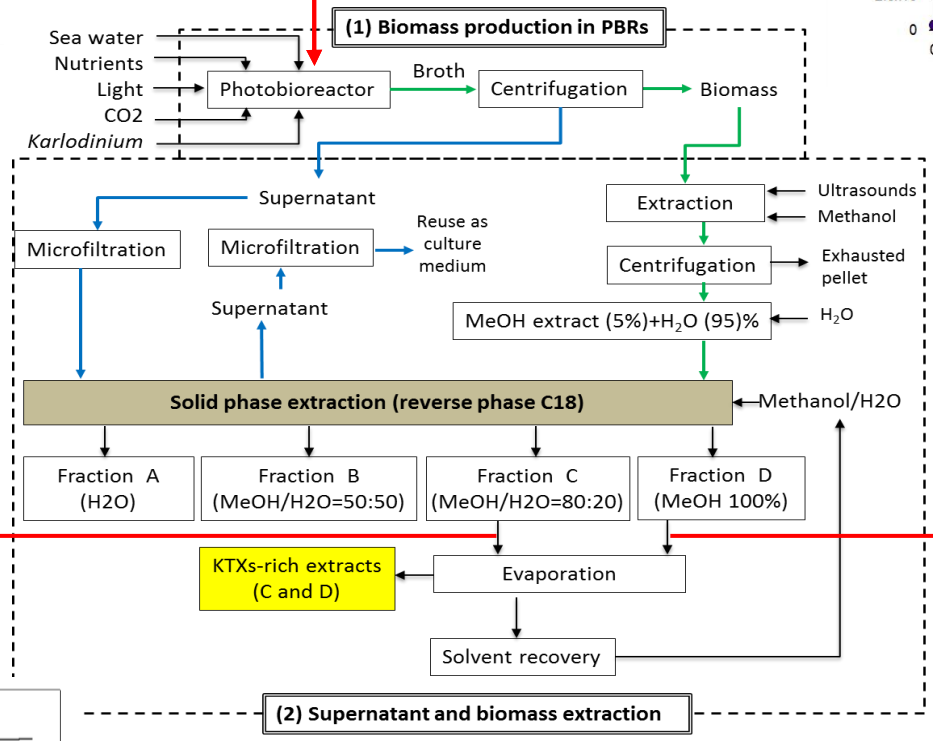

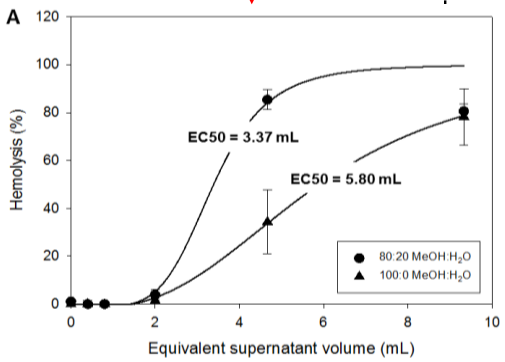

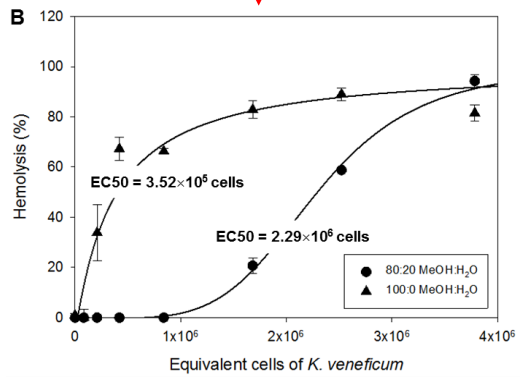

Abstract

A pilot-scale bioprocess was developed for the production of karlotoxin-enriched extracts of the marine algal dinoflagellate *Karlodinium veneficum*. A bubble column and a flat-panel photobioreactors (80–281 L) were used for comparative assessment of growth. Flow hydrodynamics and energy dissipation rates (EDR) in the bioreactors were characterized through robust computational fluid dynamic simulations. All cultures were conducted monoseptically outdoors. Bubble column (maximum cell productivity in semicontinuous operation of 58×10^{3} cell mL^{-1} day^{-1}) proved to be a better culture system for this alga. In both reactors, the local EDR near the headspace, and in the sparger zone, were more than one order of magnitude higher than the average value in the whole reactor (= 4×10^{-3} W kg^{-1}). Extraction of the culture and further purification resulted in the desired KTXs extracts. Apparently, the alga produced three congeners KTXs: KmTx-10 and its sulfated derivative (sulfo-KmTx-10) and KmTx-12. All congeners possessed hemolytic activity.

Keywords: Dinoflagellates; Microalgae; *Karlodinium veneficum*; Karlotoxin; Computational fluid dynamics; Photobioreactors

Nomenclature

CFD	Computational fluid dynamics
d_o	Nozzle hole diameter (m)
d_C	Bubble column diameter (m)
E	Energy dissipation rate due to turbulence (W kg^{-1})
EC50	Supernatant volume or cell number necessary to produce a 50% lysis of erythrocytes (mL or cell mL^{-1})
E_{spar}	Average energy dissipation rate in the vicinity of the sparger (W kg^{-1})
E_{surf}	Average energy dissipation rate at the surface of the dispersion (W kg^{-1})
E_{whole}	Average energy dissipation rate in the whole gas-liquid dispersion (W kg^{-1})
F_m	Maximum chlorophyll a fluorescence (-)
F_v	Variable chlorophyll a fluorescence (-)
H	Gas-free liquid height (m)
HRIC	High Resolution Interface Capture scheme
I_0	Incident irradiance on the reactor surface (µE m^{-2} s^{-1})
KTX	Karlotoxin
LDH	Lactate dehydrogenase
LSCBG	Least Square Cell Based for Gradient of variables in CFD simulations
N	Cell concentration (cell mL^{-1})
N_0	Initial cell concentration (cell mL^{-1})
N_i	Cell concentration at time t_i (cell mL^{-1})
NAD^+	Oxidized form of nicotinamide adenine dinucleotide
NADH	Nicotinamide adenine dinucleotide
P_i	Cell productivity at time t_i (cell mL^{-1} day^{-1})
QUICK	Quadratic Upstream Interpolation for Convective Kinematics

SIMPLE	Semi-Implicit Method for Pressure Linked Equations
t_0	Initial time (day)
t_i	Time (day)
U_b	Bubble rise velocity (m s^{-1})
U_{sg}	Superficial gas velocity based on reactor cross-sectional area (m s^{-1})
ε_{av}	Average volume fraction of gas in dispersion (-)

1. Introduction

Marine dinoflagellate microalgae produce many potentially useful bioactive compounds (Garcia Camacho et al., 2007; Kobayashi and Kubota, 2010; Gallardo-Rodríguez et al., 2012a; Wang et al., 2015). *Karlodinium veneficum* produces karlotoxins (KTXs), a group of toxins with hemolytic, cytotoxic and ichthyotoxic activity (Van Wagoner et al., 2008; Bachvaroff et al., 2009; Place et al., 2012). KTXs are polyketide toxins. Toxicity of KTXs results from their ability to form pores in cell membrane causing a loss of osmotic balance and cell death (Waters et al., 2010). KTXs are potentially useful in studies of drug designs for lowering cholesterol or targeting cancer cells high in cholesterol (Waters et al., 2010).

Only a few of dinoflagellate toxins are available commercially in small quantities mainly as calibration standards and at prohibitive prices (Gallardo-Rodríguez et al., 2012a). One hurdle to production of large amounts of bioactives is a lack of established methods for growing dinoflagellates in industrial-scale photobioreactors because of their extreme susceptibility to damage by turbulence and other hydrodynamic forces (Gallardo-Rodríguez et al., 2009; Gallardo-Rodríguez et al., 2012b; García-Camacho et al., 2014). This feature of dinoflagellates contrasts sharply with the other microalgae that are commonly grown in large-scale commercial culture systems (Contreras et al., 1999; Molina Grima et al., 1999; Sánchez Mirón et al., 1999; Sánchez Mirón et al., 2002; García Camacho et al., 2011). In earlier studies, dinoflagellates were almost always grown in indoor laboratory-scale photobioreactors (García Camacho et al., 2011; López-Rosales et al., 2015a; García-Camacho et al., 2016; López-Rosales et al., 2016). For example, a small bench-scale (≤4 L) bubble column and a larger 80 L bubble column were reported for indoor culture of *K. veneficum* (López-Rosales et al., 2015a; López-Rosales et al., 2016). The only previous outdoor cultures of this dinoflagellate used a production volume of 35 L (Fuentes-Grünewald et al., 2012), less than

50% of the photobioreactor volume used in the present work. Inclined bubble columns were used in the earlier study (Fuentes-Grünewald et al., 2012). Outdoor culture in larger (>35 L) pilot-scale photobioreactors has not been reported.

This work reports on pilot-scale (80–281 L) outdoor culture of the dinoflagellate *K. veneficum* in bubble column and flat-panel types of photobioreactors. A conventional bubble column is a relatively tall cylindrical vessel in which the culture is mixed exclusively by the action of air, or other gas, sparged at the bottom of the liquid pool. A flat-panel photobioreactor is essentially a bubble column with a rectangular cross-section. Typically, for a given volume of culture, a flat-panel photobioreactor system provides much greater surface area for capturing light compared to a cylindrical bubble column.

Outdoor photobioreactors rely on natural sunlight for photosynthesis. This work demonstrates successful pilot-scale outdoor culture of *K. veneficum* in large (≥80 L) vertical bubble column and flat-panel photobioreactors. Aseptic operation was used as production of KTXs for medical investigational purposes requires the use of a well-defined pure culture. As toxin productivity and growth of diverse dinoflagellates are strongly influenced by nutrition (Dagenais-Bellefeuille and Morse, 2013; López-Rosales et al., 2013), a culture medium specifically developed for production of KTXs by *K. veneficum* (López-Rosales et al., 2015b) was used. The culture systems were designed and compared using the energy dissipation rate fields obtained by computational fluid dynamics (CFD) simulations. The CFD-based design of pilot-scale photobioreactors for dinoflagellate culture has not been previously reported. The operating conditions used for culture assured that the hydrodynamic stresses remained below the previously established damaging threshold for *K. veneficum* (López-Rosales et al., 2015a). The bubble column proved to be the best culture system. It could be operated in a semicontinuous mode with a maximum cell productivity of 58×10^3 cell mL^{-1} day^{-1}, a value quite close to the highest values previously obtained in laboratory-scale cultures (López-

Rosales et al., 2015a; López-Rosales et al., 2016). In the flat panel photobioreactor a semicontinuous operation proved impossible and the cells suffered photoinhibition as evidenced by chlorophyll a fluorescence data. The culture broth was used to produce KTX-rich extracts using a reverse-phase chromatographic purification process.

2. Materials and methods

2.1. Microalga

The marine shear-sensitive microalgal dinoflagellate *Karlodinium veneficum* (strain K10) was used. This alga had been obtained from the Culture Collection of Harmful Microalgae of IEO, Vigo, Spain. Inocula were grown in shake flasks at 21±1 °C under a 12:12 h light–dark cycle. Four 58 W fluorescent lamps were used for illumination and the irradiance at the surface of the culture flasks was 300 μE $m^{-2}s^{-1}$. L1 medium (Guillard and Hargraves, 1993) prepared using filter-sterilized (0.22 μm Millipore filter; Millipore Corporation, Billerica, MA, USA) Mediterranean Sea water was used to grow the cultures unless specified otherwise.

2.2. Photobioreactors

Two types of photobioreactors were used: a bubble column and a rectangular flat-panel device. The bubble column consisted of a clear plastic (polymethyl methacrylate) cylindrical tube with a wall thickness of 3.3 mm. The vessel had an internal diameter (d_C) of 0.242 m. The gas-free liquid height (H) was 1.86 m. The working volume was 80 L. The culture was mixed by sparging the vessel with sterile filtered air. A nozzle with a 12 mm diameter hole (d_o) was used for sparging. The sparger nozzle extended into the vessel a distance of 20 mm from the base. The temperature was controlled by circulating chilled water through an internal steel tubing as previously reported (López-Rosales et al., 2016). The

148 configuration of the bubble column complied with the earlier published (López-Rosales et al.,
149 2015a) criterion ($H > 1.25$, $d_C/d_o \approx 20$) for assuring a sublethal hydrodynamic stress level for
150 the alga so long as the superficial aeration velocity in the vessel remained below 1.1×10^{-3} m
151 s^{-1} (equivalent to an air flow rate of 3 L min^{-1}). The actual air flow rate was 3 L min^{-1},
152 corresponding to aeration velocity of 0.444 m s^{-1} at the sparger nozzle.

153 The flat-panel system consisted of a flat-bottomed disposable polyethylene plastic bag
154 held in a rectangular iron frame as described previously (Sierra et al., 2008). The width of the
155 flat-panel device was 0.09 m and the length was 2.4 m. The gas-free culture height was 1.3 m
156 and the volume was 281 L. The thickness of the polyethylene film used in making the bag
157 was 0.75 μm and its transparency index was 0.95 in the photosynthetically active spectrum
158 (400–700 nm). The sparger consisted of a single row of 17 nozzles (4 mm hole diameter each)
159 located at the bottom of the bag. The spacing between nozzles was 0.14 m. Each nozzle
160 extended into the reactor a distance of 20 mm from the base. Each nozzle was individually
161 supplied with air. The air flow rate in each nozzle was 0.52 L min^{-1}, corresponding to air
162 velocity of 0.7 m s^{-1} at the hole. The superficial air velocity in the vessel was 6.9×10^{-4} m s^{-1}.

163 The heat exchange mechanism of the flat-panel system comprised of four 2 m long
164 stainless steel tubes (diameter = 0.025 m) located in the bag 0.5 m above the gas sparger. The
165 flat-panel photobioreactor was essentially a bubble column with a rectangular cross section.
166 Its configuration (i.e. H = 1.3 m, $d_C/d_o \approx 22.5$; here d_C was taken to be the width (= 0.09 m) of
167 the rectangular channel) complied with the criterion that was previously shown (López-
168 Rosales et al., 2015a) to limit the hydrodynamic stresses to below the damaging threshold for
169 the alga so long as the superficial aeration velocity in the vessel remained below 1.1×10^{-3} m
170 s^{-1}.

171

172 *2.3. Photobioreactor cultures*

All photobioreactor cultures were carried out outdoors at University of Almería, Spain (36.83° N, 2.40° W) during May and June. Cultures were grown photoautotrophically. Both bubble column and the flat-panel photobioreactors were used in different experiments. The dissolved oxygen concentration was monitored online as an indicator of the photosynthetic activity. The pH was controlled at pH 8.5 by automatically injecting carbon dioxide in response to a signal from the pH controller. The culture temperature was controlled at 21±1 °C by circulating thermostated water through a stainless steel tubular loop located inside each photobioreactor vessel.

Prior to use, the photobioreactors were sterilized by filling the vessels and associated pipework with filtered seawater, adding commercial bleach (~3 mL per L of water), mixing gently and letting stand (no mixing or aeration) for several hours. During this treatment, the photobioreactors were covered with a dark plastic sheet to prevent direct exposure of the bleaching solution to sunlight. Once the treatment had completed, the bleach was neutralized by adding a solution of sodium thiosulfate (250 g sodium thiosulfate ($Na_2S_2O_3 \cdot 5H_2O$) dissolved in 1 L of water; 1 mL of this solution was added for each 4 mL of the bleach used).

The bubble column contained 65 L of fresh medium and 15 L of inoculum was added. The flat-panel system contained 216.4 L of fresh medium and 64.4 L of inoculum. All inocula comprised of cells in the late exponential phase of growth. A previously optimized culture medium (López-Rosales et al., 2015b) was used in both photobioreactors. Nitrogen was supplied using $NaNO_3$ (6300 µM) and the sources of phosphorous were $Na_2HPO_4 \cdot 2H_2O$ (115.2 µM) and $C_3H_7Na_2O_6P \cdot 5H_2O$ (99.2 µM). The N:P mole ratio was 29:1. The cell concentration in a freshly inoculated photobioreactor was around 30×10^3 cells mL^{-1}. Both photobioreactors were initially operated in a batch mode. Any photoinhibition effect in this early stage of growth was minimized by covering the photobioreactors with shadow nets with a 40% attenuation of sunlight.

In the bubble column, the shadow net was removed once the biomass concentration had exceeded 200×10^3 cells mL^{-1}. In the flat-panel system the culture channel was relatively thin and the shadow net was removed once the biomass concentration had exceeded 600×10^3 cells mL^{-1}. A semicontinuous operation was explored in the bubble column at a low average dilution rate of 0.044 ± 0.01 day^{-1} because nutrient limited slow growth of *K. veneficum* was previously shown to significantly increase the cellular quota of karlotoxins (Fu et al., 2010; Van de Waal et al., 2014). Thus, around 25% of the culture volume (i.e. 20 L) was removed and replaced with an equal volume of the fresh medium. This was done on days 19, 24 and 31. Each time, the fresh medium was supplemented with phosphate and nitrate stock solutions so that the final concentrations of these nutrients in the culture were close to the values reported earlier for the optimized medium formulation (López-Rosales et al., 2015b). The other remaining nutrients were fed in proportion to the phosphate fed. The flat-panel photobioreactor was operated in a fed-batch mode (pulse feeding of phosphate and nitrate stock solutions) so that the concentrations of phosphate and nitrate in the culture medium just after each pulse were close to the values reported earlier for the optimized medium formulation (López-Rosales et al., 2015b). The other remaining nutrients were fed in proportion to the phosphate fed.

2.4. Flow cytometric measurements

A Cell Lab Quanta SC flow cytometer (Beckman Coulter Inc., Brea, CA, USA) was used to quantify the cell number concentration (N) in the cultures. At least 60,000 cells were counted per sample. Triplicate samples were measured and the data were averaged. The flow rate was kept at a moderate setting (data rate = 600 events s^{-1}) to prevent interference between cells.

The cell productivity, P_i, at a given culture time, t_i, was calculated using the following equation:

$$P_i = \frac{N_i - N_0}{t_i - t_0} \quad (1)$$

where N_i and N_0 were the cell concentrations (cells mL^{-1}) at times t_i and t_0 (day), respectively.

2.5. Photosynthetic efficiency

The maximum photochemical quantum yield of photosystem II (i.e. F_v/F_m) is a measure of the stress on the microalgal cells. F_v/F_m ratio was measured using a pulse amplitude modulation chlorophyll fluorometer (Mini-PAM-2500; Heinz Walz GmbH, Effeltrich, Germany) as described previously (López-Rosales et al., 2015a).

2.6. Determination of cell lysis

Lysis of algal cells releases the cytoplasmic enzyme lactate dehydrogenase (LDH) in the culture medium. LDH catalyzes the conversion of lactate to pyruvate and in the process reduces NAD^+ to NADH. The associated color change can be observed spectrophotometrically and is an indicator of the amount of LDH in the medium and, therefore, of the extent of cell lysis. This method has been previously used to quantify cell lysis of dinoflagellates (Gallardo-Rodríguez et al., 2015). The factors contributing to cell lysis include apoptosis and necrosis associated with external hydrodynamic forces.

2.7. Determination of phosphate and nitrate concentrations

Phosphorous species were measured as phosphate $\left(PO_4^{3-}\right)$ and nitrogen was measured as nitrate $\left(NO_3^-\right)$. These species were measured using well-established methods (Clesceri et al., 1998).

2.8. KTXs recovery

Karlotoxins (KTXs) excreted by the cells in the culture broth are easily recovered from the cell-free filtrate (Bachvaroff et al., 2008), but some KTXs remain within the cells. Accordingly, KTXs were recovered separately from the cell-free culture broth as well as the biomass of the culture samples. The cells were separated from the culture medium by continuous-flow centrifugation (RINA, model 100M/200SM, Spain) at a flow rate of 10 L h^{-1} (1800 × g). The supernatant was filtered through a membrane filter (0.22 μm pore size). The clarified supernatant was passed through a C18 flash chromatography column (40–60 μm particle size, 6 nm pore size, 80 g total packing; Bonna-Agela Technologies Inc., www.bonnaagela.com; catalog no. CO140080-0) to adsorb the KTXs. Prior to use, the C18 column had been equilibrated with methanol and then with distilled water. The KTXs were loaded on the C18 column at a flow rate of 1.2 L h^{-1}. Afterwards, the KTXs were eluted from the column using a step gradient of 1.2 L of each of the following solvents: pure water, 50% aqueous methanol, 80% aqueous methanol and pure methanol. Each methanolic fraction was collected separately and tested for hemolytic activity.

The wet algal biomass pellet recovered after the above mentioned centrifugation step was resuspended in methanol (450 mL) and sonicated using an ultrasonic probe-type device (UP200S, Hielscher Ultrasonics™; 200 W, 24 kHz, 4 min). The sonication power was 50% of full power and the pulse control was set at 0.5. This sonicated suspension was centrifuged (1831 × g, 10 min, 10 °C), the methanolic supernatant was recovered and filtered (0.22 μm pore size membrane filter) to remove cell debris. The clarified supernatant was diluted with HPLC-grade water to reduce the concentration of methanol to below 20% v/v. The KTXs in this solution were recovered by flash chromatography exactly as described above for the supernatant of the culture broth. The overall process flow scheme used for biomass production and recovery of KTXs-rich extracts is shown in Fig. 1.

2.9. Hemolytic activity

The KTXs content in each of the above-mentioned aqueous methanolic fractions were measured in terms of the percentage hemolytic activity relative to a positive control. Sheep blood erythrocyte lysis assay was used, as described elsewhere (Riobó et al., 2008). Specified volumes of the various aqueous methanolic fractions were placed in microwells of a microtiter plate and air-dried. Each tested volume corresponded to either an equivalent volume of the culture supernatant, or an equivalent number of algal cells if the tested volume came from the biomass pellet. Erythrocytes from defibrinated sheep blood were used at a concentration of 45×10^6 cells per well. Erythrocytes incubated in Mediterranean Sea water served as negative controls. Positive control, or 100% hemolysis, was obtained using distilled water. The measured hemolysis data were used to determine the EC50 value, that is the equivalent supernatant volume, or equivalent cell number, needed to produce 50% hemolysis. Triplicate samples were measured and average values are reported.

2.10. Characterization of KTXs

The semi-purified fractions of KTXs were further enriched and characterized by LC–MS/MS and NMR as described by Waters et al. (2015).

2.11. Computational fluid dynamics (CFD)

Computational fluid dynamic simulations were used to characterize the flow and map the local energy dissipation rates (E) in various zones of the photobioreactors. The geometry and the aeration rates for the two bioreactors were given in an earlier part of this paper.

The time-dependent simulations were performed using ANSYS Fluent® v16.2 (www.ansys.com) software. An implicitly formulated Eulerian two-phase model was used to

describe the gas-liquid interactions. The liquid velocity at the solid walls was taken to be zero (i.e. non-slip condition). In all simulations the continuous phase was seawater (density = 1023 kg m^{-3}, viscosity = 1.28×10^{-3} Pa s) and the dispersed phase was air (density = 1.225 kg m^{-3}, viscosity = 1.789×10^{-5} Pa s). Viscosity of the freshly inoculated culture was the same as the viscosity of seawater. No measureable changes in viscosity were detected during culture. Therefore, the viscosity of seawater was used in all simulations. The drag between phases was estimated using the Grace model. A surface tension value of 71.8×10^{-3} N m^{-1} was used. The bubble diameter was estimated according to Jamialahmadi et al. (2001). The mean bubble diameter was 15 mm in the bubble column and 8.9 mm in the flat-panel photobioreactor.

The outlets of the bioreactors were modeled as pressure outlets with an air volume fraction of 1. The air inlets were modeled as velocity inlets using the velocities specified earlier, with an air volume fraction of 1. Simulations used a pressure-based model under transient conditions. Gravity was included in the model in the negative *z*-direction for the bubble column and negative *y*-direction for the flat-panel system. The other settings were as follows: SIMPLE for the pressure-velocity coupling; Least Square Cell Based for Gradient (LSCBG) scheme for spatial discretization; QUICK for momentum; modified HRIC for volume fraction; and Second Order Upwind for turbulent kinetic energy and dissipation rate.

For the bubble column, the time step size was fixed at 1×10^{-4} s with a maximum of 20 iterations per time step. Once the flow had stabilized, the data were time averaged for 30 s with a data sampling interval of 0.01 s. The optimal mesh size in the bubble column was 5.53×10^{5} elements with the element size ranging from 1 to 7 mm. All simulations for the bubble column used an air-free culture height of 1.86 m.

The flow in the flat-panel photobioreactor was simulated exactly as explained for the bubble column, except for the following. Separate flow simulations were carried out for the air-free culture heights of 1.3 m and 0.65 m. In both cases, the time step size was fixed at

1×10^{-3} s with a maximum of 20 iterations per time step. Once the flow had stabilized, the data were time averaged for 30 s with a data sampling interval of 0.01 s. The optimal mesh size in the system with a static culture height of 1.3 m was 4.09×10^{5} elements with the element size ranging from 0.6 to 10 mm. For the flat-panel system with a gas-free culture height of 0.65 m, the optimal mesh size was 3.17×10^{5} elements with the element size ranging from 0.57 to 9 mm.

The flow in the flat-panel photobioreactor was simulated for the two gas-free culture heights for the following reason: Based on an analysis published earlier (López-Rosales et al., 2015a), a vessel filled to 1.3 m should not produce strong enough hydrodynamic stresses to damage cells at the aeration rate used in the present study. In contrast, at the same aeration rate, a vessel filled to ≤0.65 m was expected to exceed the cell damage threshold hydrodynamic stress (López-Rosales et al., 2015a). In all three cases simulated, the convergence criteria were the same: a residuals value of 10^{-5} for all variables.

3. Results and discussion

3.1. CFD simulations

Both bubble column and the flat-panel bioreactors operated well within the bubble flow regime (superficial air velocity << 0.05 m/s) in which, away from the sparger, the gas bubble rise as individual bubbles without interacting (Chisti, 1989). The hydrodynamics in these reactors are discussed separately in the following sections.

3.1.1. Bubble column

Time-averaged gas holdup and the local specific energy dissipation rates in different zones of the bubble column are shown in Fig. 2A–C. The simulated air holdup was 0.22% and the experimental holdup was 0.27%. The gas plume from the sparger rose up vertically. The

gas holdup in the plume was higher than in the surrounding fluid. The liquid moved up with the bubbles in the air plume and sank down along the column walls (Fig. 2D, E). This downflow was symmetrical on all sides as there was no evidence of the gas plume being distorted in any particular direction. The liquid downflow velocity vectors along the column wall are clearly seen in Fig. 2D. A magnified image (Fig. 2E) shows that the liquid downflow along the walls did not all reach the bottom, but short circuited into up flowing liquid in the vicinity of the gas plume to rise with the liquid in this zone. The zones of highest specific energy dissipation occurred on the upper surface of the fluid where bubbles ruptured and near the gas plume emerging from the sparger (Fig. 2B, C). The energy dissipated in these zones apparently was insufficient to damage cells as discussed later in this paper in the context of the biomass growth studies.

3.1.2. Flat-panel system

Simulations confirmed that the air plumes near the center of the reactor ascended straight up without interacting (Fig. 3A, B). Liquid was carried up in the wakes behind rising bubbles in the gas plumes. Eventually this liquid returned from the surface to the bottom of the reactor. Near the ends of the reactor, adjacent to the shorter walls, the confining walls forced the liquid to flow inwards toward the plumes. This distorted the rising air plumes close to the two small side walls. Thus, the four air plumes closest to the side walls near both ends of the taller reactor (Fig. 3A) and three air plumes next the side walls in the smaller reactor (Fig. 3B) were distorted. Consistent with this, large liquid circulation zones were clearly visible in the time-averaged seawater velocity vector images of the simulations (Fig. 3C, D). Circulation cells were much larger in the taller reactor (Fig. 3C) compared to the shorter vessel (Fig. 3D). In any vessel, the circulation cells at the opposite ends were symmetrical (Fig. 3C, D).

For identical values of the superficial air flow rates, the gas holdup was higher in the shorter reactor (gas-free liquid height = 0.65 m) compared to the taller reactor (Fig. 3A, B). A flat-panel reactor is essentially a bubble column with a rectangular cross-section. According the well-established theory, in a bubble column the gas holdup (ε_{av}) at steady state equals the ratio of the superficial air velocity (U_{sg}) and the average bubble rise velocity (U_b) (Chisti, 1989), i.e. $\varepsilon_{av} = U_{sg}/U_b$. Therefore, the average bubble rise velocity in the shorter reactor was smaller than in the taller reactor. This implied a smaller bubble diameter in the shorter reactor, although the initial estimates for bubble size were the same for both the flat-panel reactors as previously noted. A smaller bubble diameter in turn implied a higher specific energy dissipation rate in the shorter reactor because energy dissipated in the fluid is responsible for the breakup of bubbles. Nearly 25% higher rates of specific energy dissipation in the shorter reactor were confirmed by simulations (Fig. 4, Table 1).

In addition to affecting the average air bubble size, the specific energy dissipation rate (E) determines the size of fluid microeddies in the reactor and this in turn determines whether algal cells are damaged by turbulence (López-Rosales et al., 2015a). The local specific energy dissipation rate at the surface (E_{surf}) of the liquid was between 6- and 8-fold the average specific energy dissipation rate (Table 1). In air-sparged bioreactors, the energy dissipation at the surface is mainly associated with the violently rupturing gas bubbles (Chisti, 2000). This intense local energy dissipation rate has often been implicated in damaging fragile cells (Chisti, 2000) including cells of dinoflagellates (Place et al., 2012; Gallardo-Rodríguez et al., 2016; López-Rosales et al., 2017). Smaller bubbles release more energy during rupture compared to larger bubbles (Chisti, 2000). However, the difference in bubble sizes in the two flat-panel systems was not large as the E_{surf} value in the taller reactor was marginally lower than in the shorter vessel (Table 1).

In both reactors, the local specific energy dissipation rate (E_{spar}) in the vicinity of gas sparger was high, between 23- and 30-fold the average energy dissipation rate (E_{whole}) (Table 1). The E_{spar} values were similar (within ±3% of the average value) for both reactors (Table 1) because the spargers and the gas flow rates were identical.

The *E* profiles (Fig. 3A, B) and values of E_{surf} and E_{spar} were similar in both reactors, therefore, the difference in the average energy dissipation rates was small, with the average dissipation rate in the shorter vessel being about 25% greater (Table 1).

3.2. Culture in outdoor photobioreactors

The cell concentration (*N*) and F_v/F_m versus time profiles for outdoor cultures are shown in Fig. 5A (for bubble column) and Fig. 5B (for flat-panel). The data shown were obtained in parallel runs during May and June. The incident solar radiation at the location of the reactors (I_o) was measured with a thermoelectric pyranometer connected to an AC-420 adapter (LP-02, Geónica S.A., Spain). Thus, the average daily value of I_o during the culture period was 2100±162 μE m^{-2} s^{-1}. The culture profiles during batch operation in the two bioreactors were similar, but not identical: the final *N* value in stationary phase in the bubble column (Fig. 5A) was a little higher than in the flat-panel system (Fig. 5B). In both cases, an initial lag phase was followed by a short exponential phase of growth and then a linear growth phase. In the bubble column, a decline phase had not set in by the time the operation was switched to the fed-batch mode. In the flat-panel device, there was a short stationary phase that led to a rapid decline phase (Fig. 5B).

Potential damage to culture by intense sunlight during the optically dilute lag phase was minimized by placing a shadow net on east and west sides (i.e. the sides facing the sun at dawn and dusk) of both types of photobioreactors. This net was removed (day 7 in bubble

column, Fig. 5A; day 11 in flat-panel, Fig. 5B) once the cells had become established and exponential growth had commenced.

Compared to the bubble column, the duration of the linear growth phase was longer in the flat-panel system. Typically, onset of linear growth is indicative of a nutrient limitation. In this work, all the inorganic nutrients were regularly fed and carbon dioxide was fed in response to a pH controller. Therefore, a light limitation and/or photoinhibition were the only explanations for the transition from exponential to linear growth. A light limitation inevitably occurs in all kinds of culture systems because a growing population of cells shades the cells in deeper parts of the photobioreactor channel. Less of a light limitation was likely in the flat-panel system compared to the bubble column, because the flat-panel device had a lower cell concentration, a shallower depth, and a bigger surface-to-volume ratio. Therefore, photoinhibition likely contributed to an early onset of linear growth. There was no evidence of any photoinhibition in the bubble column (diameter = 0.242 m), but photoinhibition did occur in the much thinner flat-panel culture system (depth = 0.09 m). Thus, values of F_v/F_m in the bubble column were mostly ≥0.5 during much of the operation (Fig. 5A) whereas these values were lower in the flat-panel bioreactor (Fig. 5B).

Although there appears to be no consensus concerning dinoflagellates, F_v/F_m values of around 0.6 are suggestive of healthy cells and lower values suggest cells under stress. Stress in the flat-panel culture system could potentially be attributed to either photoinhibition in a relatively shallow channel, or hydrodynamic factors, or a combination of these. Hydrodynamic factors could not be excluded because the depth of the culture (= 1.3 m) in the flat-panel device was close the threshold depth (= 1.25 m) that needs to be exceeded to prevent hydrodynamic damage to *K. veneficum* in bubble columns (López-Rosales et al., 2015a). During entire operation, unusually high concentrations of the cytosolic enzyme LDH were measured in the culture supernatant in the flat-panel system compared to the bubble

columns. This was indicative of cell lysis that can arise both due to strong photoinhibition and/or through cell damage caused by hydrodynamic stresses.

Overall, the batch culture in the relatively optically thick (diameter = 0.242 m) bubble column performed better compared to the flat-panel bioreactor (channel width = 0.09 m). The maximum specific growth rate in the bubble column during exponential growth was 0.320 day^{-1} on day 3.26 of culture and the final cell concentration in batch mode of operation was 1×10^{6} cells mL^{-1}. This cell concentration was similar to the values obtained with this medium formulation in laboratory-scale bubble columns (López-Rosales et al., 2015b), demonstrating a satisfactory scale-up of the culture system. In contrast with this, in the flat-panel photobioreactor the maximum specific growth rate (exponential growth) was 0.246 day^{-1} on day 6.42 of culture. The specific growth rate in the bubble column was nearly 30% higher than 0.25 day^{-1} reported by Fuentes-Grünewald et al. (2012).

The values of peak cell productivity were identical (= 57×10^{3} cell mL^{-1} day^{-1}) in batch operations in both photobioreactors despite a much large surface-to-volume ratio of the flat-panel system. The above noted peak cell productivity was comparable to data reported earlier in the same cylindrical bubble column operated indoors using light emission diodes (LED) for illumination (López-Rosales et al., 2016).

On day 19, the operational mode of the bubble column was switched to a semicontinuous operation (Fig. 5A). A maximum cell productivity of 58×10^{3} cell mL^{-1} day^{-1} was attained Fig. 5A). This value was essentially the same as the peak productivity attained in the batch mode of operation, but it occurred at a higher cell concentration (Fig. 5A). *K. veneficum* could be cultured stably in a semicontinuous operation, unlike the culture collapse reported for the dinoflagellate *Azadinium spinosum* during semicontinuous culture in a bubble column (Jauffrais et al., 2012).

3.3. Production of a KTXs-rich methanolic extract

Of the solvent fractions collected from the C18 chromatography column, only the 80% methanolic fraction and the 100% methanolic fraction had detectable hemolysis activity (Van Wagoner et al., 2010). The percent hemolysis (i.e. the percentage of the erythrocytes lysed) and EC50 values (culture supernatant volume equivalent for achieving 50% hemolysis, or algal cell number equivalent for achieving 50% hemolysis) for these methanolic fractions are shown in Fig. 6.

Based on the data, the 80% methanolic fraction recovered most of the KTXs that were adsorbed from the cell-free culture supernatant (Fig. 6A) whereas the 100% methanolic fraction recovered most of the KTXs adsorbed from extracts of the biomass (Fig. 6B). These results are consistent with studies reported using other strains of *K. veneficum* (Kempton et al., 2002; Place and Deeds, 2005; Bachvaroff et al., 2008). The results suggest differences in hydrophobicities of the KTXs released in the extracellular culture fluid compared to the KTXs retained within the cells. Therefore, the cells produced at least two variants of KTXs (Van Wagoner et al., 2010) having different hydrophobicities due to differences in the variable functional groups (e.g. sulfation of the core molecule) in the molecules. The relatively more hydrophobic KTXs would desorb with pure methanol and, therefore, these must have predominated in the extract of the algal cells.

3.4. Characterization of the KTXs

Multiple types of KTXs are known to occur (Place et al., 2012; Waters et al., 2015). All of them have the same basic structure but differ in the number of carbons in the main carbon backbone and the nature of certain functional groups in the molecule. Based on a preliminary analysis from the LC-MS/MS and NMR data, the KTXs produced by *K. veneficum* in this work belonged to the KTX-2 group with a terminal chlorine. Specifically,

three congeners KmTx-10, sulfo-KmTx-10 and KmTx-12 (low abundance) were detected and purified.

3.5. Future prospects

In principle, the bioprocess developed in this work can be extended to production of bioactives from other shear-sensitive dinoflagellates. A bubble column type of outdoor culture system can be effectively used up to a working volume of at least 80 L to grow a shear-sensitive dinoflagellate such as *K. veneficum*. For this dinoflagellate, any further scale up of production must rely on multiplying the number of photobioreactors. The downstream extraction-purification steps of the KTX process can be easily scaled-up to a multi-kilogram level as commercial chromatographic separations technology applicable to this scale is already in use in other biotechnology processes (Chisti, 2008). The bioprocess developed in the present work, used only readily accessible and inexpensive materials and solvents to minimize the cost of production. The process is therefore both technically and economically practicable.

4. Conclusions

Outdoor production of *K. veneficum* and KTXs in pilot-scale bubble column and flat-panel photobioreactors was compared. Overall, the bubble column was a better culture system for use with this alga. The height of the culture fluid and the maximum air flow rate had to be carefully selected to minimize turbulence-associated damage to cells of this highly shear-susceptible alga. The alga could be grown in batch, semicontinuous and fed-batch operations. The KTXs were readily recovered by conventional column chromatography from large volumes of the culture broth. The alga produced at least three variants of KTXs.

Acknowledgements

This research was funded by the Spanish Ministry of Economy and Competitiveness (Grants SAF2011-28883-C03-02 and CTQ2014-55888-C3-02) and the European Regional Development Fund Program. This research was funded in part by grants from OHH NIHR01ES021949-01/NSFOCE1313888 and NOAA-NOS-NCCOS-2012-2002987 to ARP.

References

1. Bachvaroff, T.R., Adolf, J.E., Squier, A.H., Harvey, H.R., Place, A.R., 2008. Characterization and quantification of karlotoxins by liquid chromatography–mass spectrometry. Harmful Algae 7, 473–484.
2. Bachvaroff, T.R., Adolf, J.E., Place, A.R., 2009. Strain variation in *Karlodinium veneficum* (dinophyceae): Toxin profiles, pigments, and growth characteristics. J. Phycol. 45, 137–153.
3. Chisti, Y., 1989. Airlift Bioreactors, Elsevier, London, pp. 355.
4. Chisti, Y., 2000. Animal-cell damage in sparged bioreactors. Trends Biotechnol. 18, 420–432.
5. Chisti, Y., 2007. Strategies in downstream processing, in: Subramanian, G. (Ed.), Bioseparation and Bioprocessing: A Handbook, second ed, vol. 1. Wiley-VCH, New York, pp. 29-62.
6. Clesceri, L.S., Greenberg, A.E., Eaton, A.D., 1998. Standard Methods for the Examination of Water and Wastewater, 20th Edition, APHA American Public Health Association.
7. Contreras, A., García, F., Molina, E., Merchuk, J.C., 1999. Influence of sparger on energy dissipation, shear rate, and mass transfer to sea water in a concentric-tube airlift bioreactor. Enzyme Microb. Technol. 25, 820–830.

8. Dagenais-Bellefeuille, S., Morse, D., 2013. Putting the N in dinoflagellates. Front. Microbiol. 4, 369.

9. Fu, F. X., Place, A. R., Garcia, N. S., Hutchins, D. A., 2010. CO2 and phosphate availability control the toxicity of the harmful bloom dinoflagellate Karlodinium veneficum. Aquat. Microb. Ecol. 59(1), 55-65.

10. Fuentes-Grünewald, C., Garcés, E., Alacid, E., Rossi, S., & Camp, J.,2012. Biomass and Lipid Production of Dinoflagellates and Raphidophytes in Indoor and Outdoor Photobioreactors. Marine Biotechnology, 15(1), 37–47.

11. Gallardo-Rodríguez, J.J., Sánchez-Mirón, A., García-Camacho, F., Cerón-García, M.C., Belarbi, E.H., Chisti, Y., et al., 2009. Causes of shear sensitivity of the toxic dinoflagellate *Protoceratium reticulatum*. Biotechnol. Prog. 25, 792–800.

12. Gallardo-Rodríguez, J., Sánchez-Mirón, A., García-Camacho, F., López-Rosales, L., Chisti, Y., Molina-Grima, E., 2012a. Bioactives from microalgal dinoflagellates. Biotechnol. Adv. 30, 1673–1684.

13. Gallardo-Rodríguez, J.J., García-Camacho, F., Sánchez-Mirón, A., López-Rosales, L., Chisti, Y., Molina-Grima, E., 2012b. Shear-induced changes in membrane fluidity during culture of a fragile dinoflagellate microalga. Biotechnol. Prog. 28, 467–473.

14. Gallardo-Rodríguez, J.J., López-Rosales, L., Sánchez-Mirón, A., García-Camacho, F., Molina-Grima, E., 2015. Rapid method for the assessment of cell lysis in microalgae cultures. J. Appl. Phycol. 28, 105–112.

15. Gallardo-Rodríguez, J.J., López-Rosales, L., Sánchez-Mirón, A., García-Camacho, F., Molina-Grima, E., Chalmers, J.J., 2016. New insights into shear-sensitivity in dinoflagellate microalgae. Bioresour. Technol. 200, 699–705.

16. Garcia Camacho, F., Gallardo Rodríguez, J., Sánchez Mirón, A., Cerón García, M.C., Belarbi, E.H., Chisti, Y., Molina Grima, E., 2007. Biotechnological significance of

toxic marine dinoflagellates. Biotechnol. Adv. 25, 176–194.

17. García Camacho, F., Gallardo Rodríguez, J.J., Sánchez Mirón, A., Belarbi, E.H., Chisti, Y., Molina Grima, E., 2011. Photobioreactor scale-up for a shear-sensitive dinoflagellate microalga. Process Biochem. 46, 936–944.

18. García-Camacho, F., Sánchez-Mirón, A., Gallardo-Rodríguez, J., López-Rosales, L., Chisti, Y., Molina-Grima, E., 2014. Culture of microalgal dinoflagellates, in: Botana, L.M. (Ed.), Seafood and Freshwater Toxins: Pharmacology, Physiology, and Detection, third ed. CRC Press, Boca Raton, pp. 551–566.

19. García-Camacho, F., López-Rosales, L., Sánchez-Mirón, A., Belarbi, E.H., Chisti, Y., Molina-Grima, E., 2016. Artificial neural network modeling for predicting the growth of the microalga *Karlodinium veneficum*. Algal Res. 14, 58–64.

20. Guillard, R.R.L., Hargraves, P.E., 1993. *Stichochrysis immobilis* is a diatom, not a chrysophyte. Phycologia 32, 234–236.

21. Jamialahmadi, M., Zehtaban, M.R., Müller-Steinhagen, H., Sarrafi, A., Smith, J.M., 2001. Study of bubble formation under constant flow conditions. Chem. Eng. Res. Des. 79, 523–532.

22. Jauffrais, T., Kilcoyne, J., Séchet, V., Herrenknecht, C., Truquet, P., Hervé, F., et al., 2012. Production and isolation of azaspiracid-1 and -2 from *Azadinium spinosum* culture in pilot scale photobioreactors. Mar. Drugs 10, 1360–1382.

23. Kempton, J.W., Lewitus, A.J., Deeds, J.R., Law, J.M., Place, A.R., 2002. Toxicity of *Karlodinium micrum* (Dinophyceae) associated with a fish kill in a South Carolina brackish retention pond. Harmful Algae 1, 233–241.

24. Kobayashi, J., Kubota, T., 2010. Bioactive metabolites from marine dinoflagellates, in: Mander, L., Liu, H.-W. (Eds.), Comprehensive Natural Products II: Chemistry and Biology, vol. 2. Elsevier, Amsterdam, pp. 263-325.

595 25. López-Rosales, L., Gallardo-Rodríguez, J.J., Sánchez-Mirón, A., Contreras-Gómez, A.,
596 García-Camacho, F., Molina-Grima, E., 2013. Modelling of multi-nutrient interactions
597 in growth of the dinoflagellate microalga *Protoceratium reticulatum* using artificial
598 neural networks. Bioresour. Technol., 146, 682–688.
599 26. López-Rosales, L., García-Camacho, F., Sánchez-Mirón, A., Contreras-Gómez, A.,
600 Molina-Grima, E., 2015a. An optimisation approach for culturing shear-sensitive
601 dinoflagellate microalgae in bench-scale bubble column photobioreactors. Bioresour.
602 Technol. 197, 375–382.
603 27. López-Rosales, L., García-Camacho, F., Sánchez-Mirón, A., Chisti, Y., 2015b. An
604 optimal culture medium for growing *Karlodinium veneficum*: Progress towards a
605 microalgal dinoflagellate-based bioprocess. Algal Res. 10, 177–182.
606 28. López-Rosales, L., García-Camacho, F., Sánchez-Mirón, A., Martín-Beato, E., Chisti,
607 Y., Molina-Grima, E., 2016. Pilot-scale bubble column photobioreactor culture of a
608 marine dinoflagellate microalga illuminated with light emission diodes. Bioresour.
609 Technol. 216, 845–855.
610 29. López-Rosales, L., García-Camacho, F., Sánchez-Mirón, A., Contreras-Gómez, A.,
611 Molina-Grima, E., 2017. Modeling shear-sensitive dinoflagellate microalgae growth in
612 bubble column photobioreactors. Bioresour. Technol. 245, 250–257.
613 30. Molina Grima, E., Acién Fernández, F.G., García Camacho, F., Chisti, Y., 1999.
614 Photobioreactors: light regime, mass transfer, and scaleup. J. Biotechnol. 70, 231–247.
615 31. Place, A., Deeds, J., 2005. Dinoflagellate karlotoxins, methods of isolation and uses
616 thereof. (2005). United States Patent Application US 2005/0209104A1.
617 32. Place, A.R., Bowers, H.A., Bachvaroff, T.R., Adolf, J.E., Deeds, J.R., Sheng, J., 2012.
618 *Karlodinium veneficum*—The little dinoflagellate with a big bite. Harmful Algae 14,
619 179–195.

620 33. Riobó, P., Paz, B., Franco, J.M., Vázquez, J.A., Murado, M.A., 2008. Proposal for a
621 simple and sensitive haemolytic assay for palytoxin. Harmful Algae 7, 415–429.
622 34. Sánchez Mirón, A., Contreras Gómez, A.C., García Camacho, F., Molina Grima, E.,
623 Chisti, Y., 1999. Comparative evaluation of compact photobioreactors for large-scale
624 monoculture of microalgae. J. Biotechnol. 70, 249–270.
625 35. Sánchez Mirón, A., Cerón García, M.-C., García Camacho, F., Molina Grima, E.,
626 Chisti, Y., 2002. Growth and biochemical characterization of microalgal biomass
627 produced in bubble column and airlift photobioreactors: Studies in fed-batch culture.
628 Enzyme Microbial Technol. 31, 1015–1023.
629 36. Sierra, E., Acién, F.G., Fernández, J.M., García, J.L., González, C., Molina, E., 2008.
630 Characterization of a flat plate photobioreactor for the production of microalgae. Chem.
631 Eng. J., 138, 136–147.
632 37. Van de Waal, D.B., Smith, V.H., Declerck, S.A., Stam, E., Elser, J.J., 2014.
633 Stoichiometric regulation of phytoplankton toxins. Ecol. Lett. 17, 736–742.
634 38. Van Wagoner, R.M., Deeds, J.R., Satake, M., Ribeiro, A.A., Place, A.R., Wright,
635 J.L.C., 2008. Isolation and characterization of karlotoxin 1, a new amphipathic toxin
636 from *Karlodinium veneficum*. Tetrahedron Lett. 49, 6457–6461.
637 39. Van Wagoner, R.M., Deeds, J.R., Tatters, A.O., Place, A.R., Tomas, C.R., Wright,
638 J.L.C., 2010. Structure and relative potency of several karlotoxins from *Karlodinium*
639 *veneficum*. J. Nat. Prod. 73, 1360–1365.
640 40. Wang, S., Chen, J., Li, Z., Wang, Y., Fu, B., Han, X., Zheng, L., 2015. Cultivation of
641 the benthic microalga *Prorocentrum lima* for the production of diarrhetic shellfish
642 poisoning toxins in a vertical flat photobioreactor. Bioresour. Technol. 179, 243–248.
643 41. Waters, A.L., Hill, R.T., Place, A.R., Hamann, M.T., 2010. The expanding role of
644 marine microbes in pharmaceutical development. Curr. Opin. Biotechnol. 21, 780–786.

645 42. Waters, A. L., Oh, J., Place, A. R., Hamann, M. T., 2015. Stereochemical studies of the
646 Karlotoxin class using NMR and DP4 chemical shift analysis and insights into their
647 mechanism of action (MoA). Angew. Chem. 127, 15931–15936.

648

649

650 **Table 1**

651 Specific energy dissipation rate values in the liquid phase for the flat-panel photobioreactor.

652

Liquid height (m)	E_{whole} (W kg^{-1})	E_{surf} (W kg^{-1})	E_{spar} (W kg^{-1})
1.30	4×10^{-3}	33×10^{-3}	121×10^{-3}
0.65	5×10^{-3}	30×10^{-3}	115×10^{-3}

653

654

655

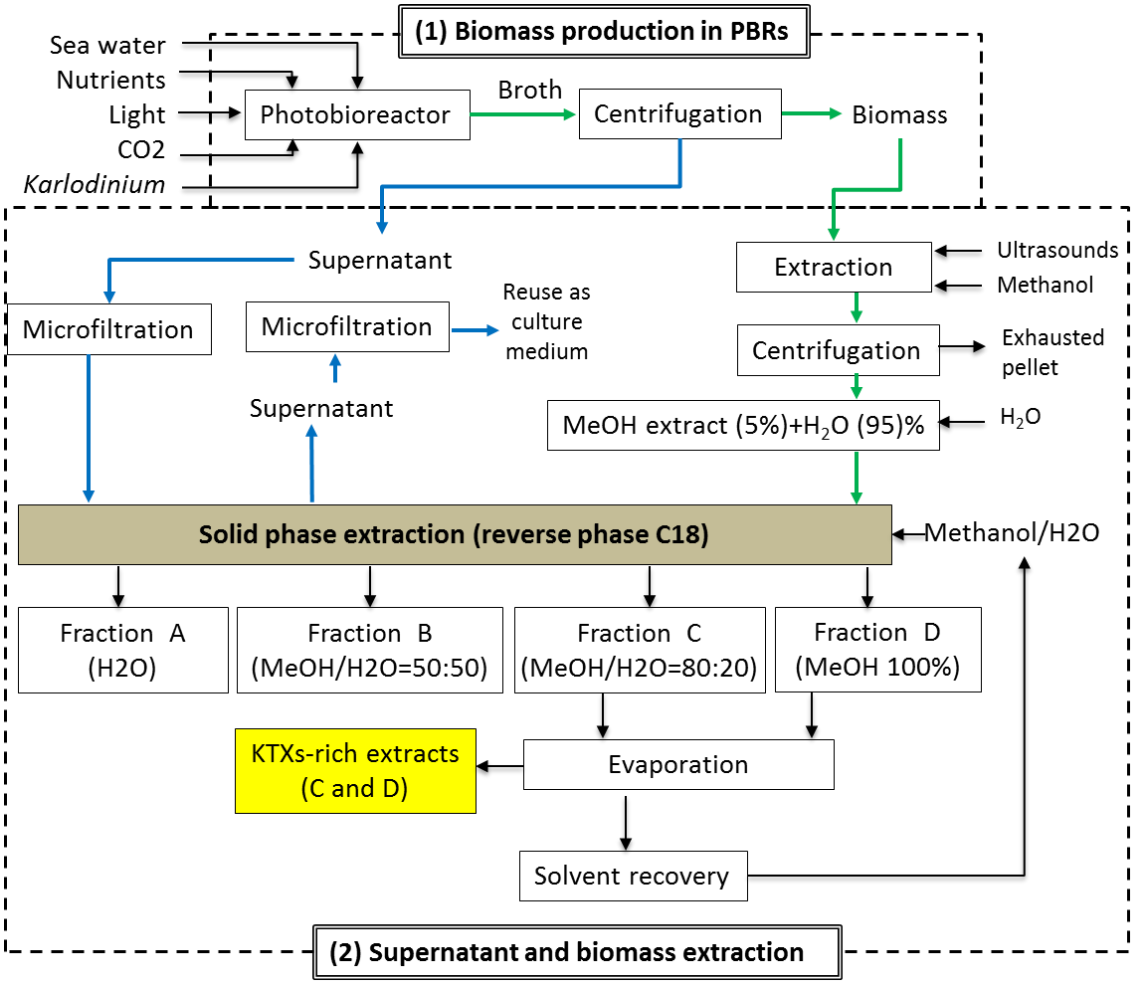

Fig. 1. Process outline for pilot-scale production of the biomass of *Karlodinium veneficum* and its KTXs-rich extracts.

656

657

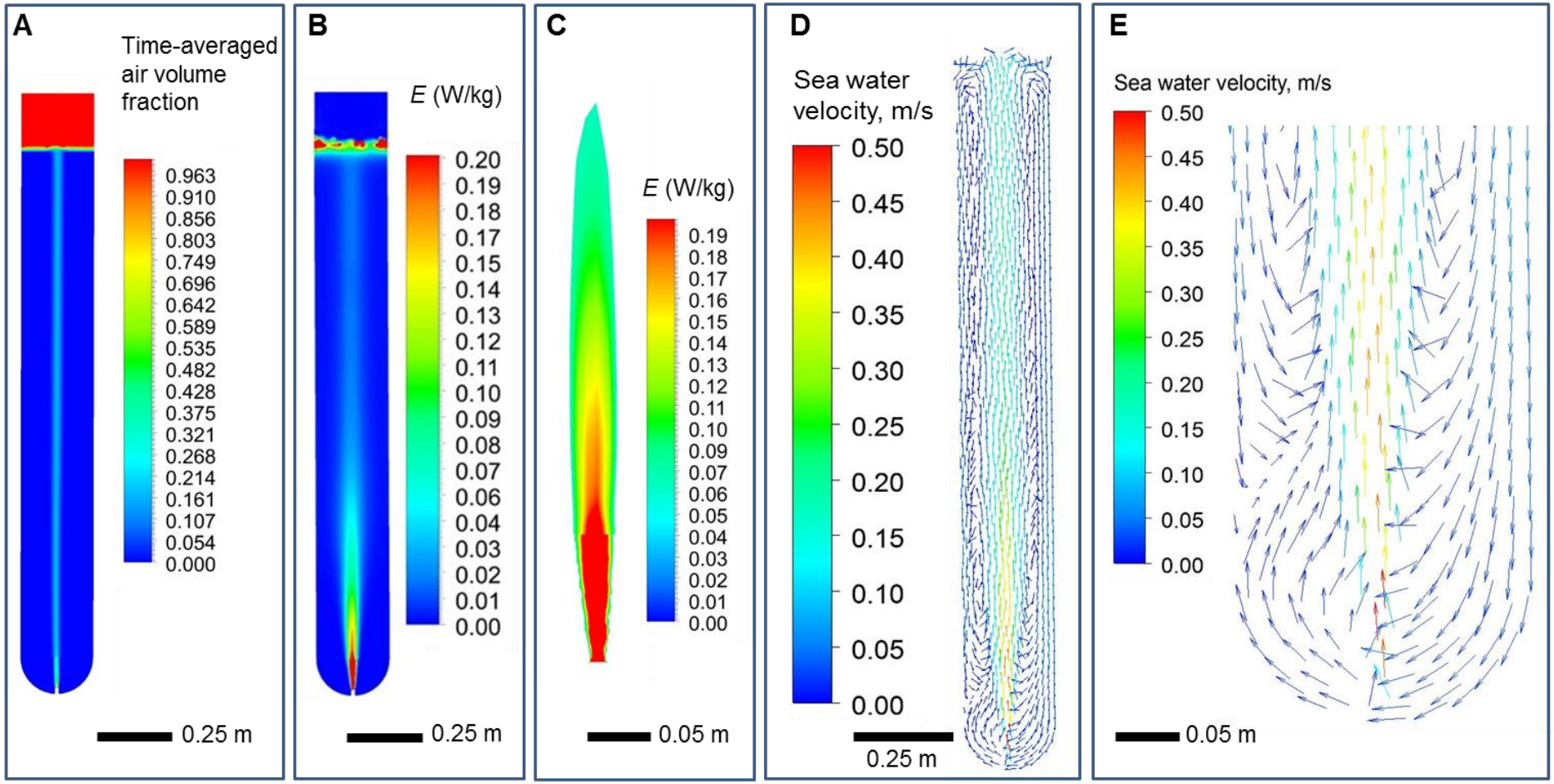

Fig. 2. Volume fraction of air (averaged over 30 s) in the bubble column (A); local energy dissipation rate *E* in the bubble column (averaged over 30 s) (B); and local energy dissipation rate near the bubble column sparger nozzle (averaged over 30 s) (C). Time-averaged (30 s) seawater velocity vectors in the entire bubble column (D) and the bottom zone of the column (E). All data are in the longitudinal *x*–*y* plane.

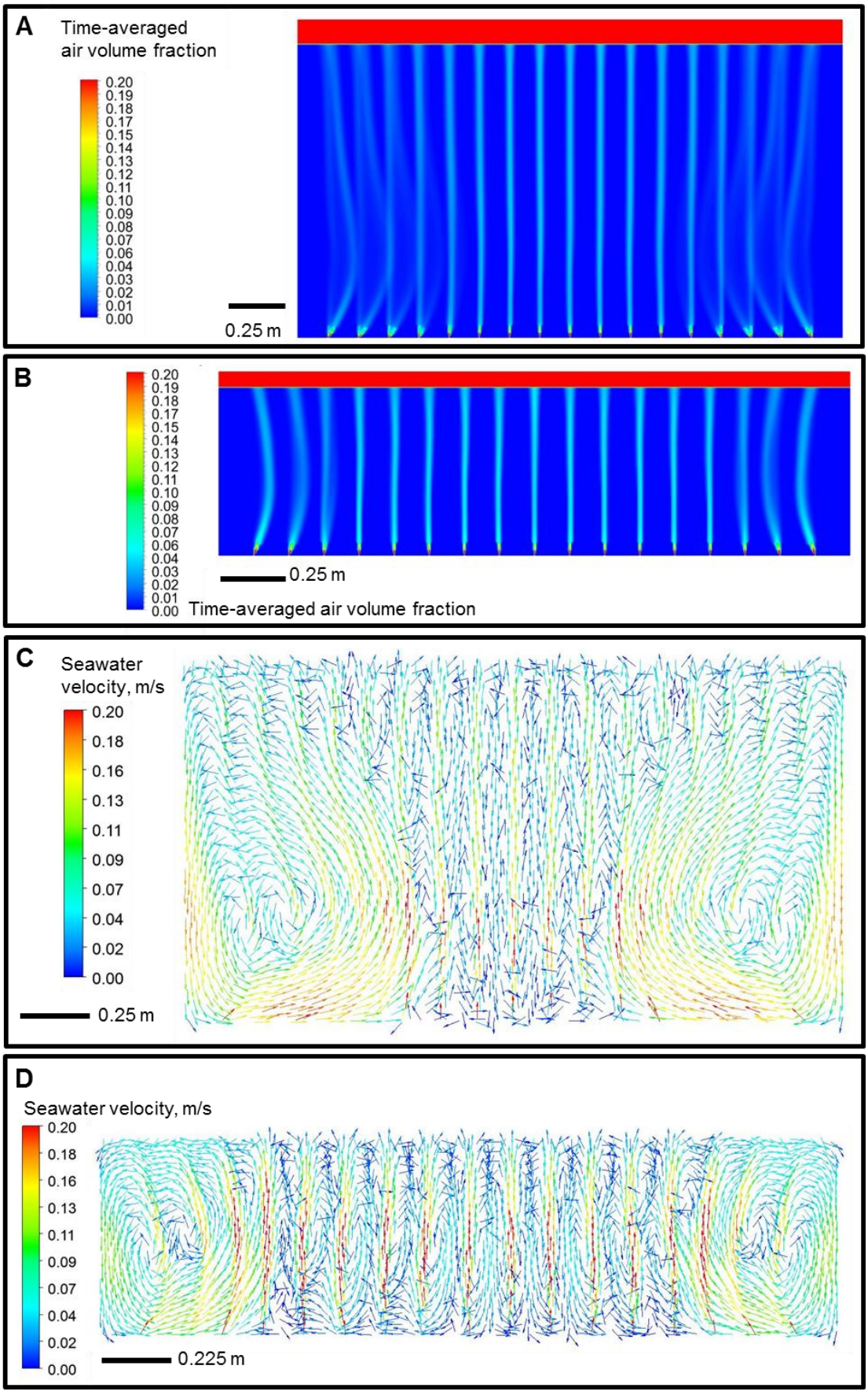

663

664

665 **Fig. 3.** Time-averaged volume fraction (ε_{av}) of air in a vertical central plane in flat-panel
666 photobioreactor with a gas-free liquid height of: (A) 1.3 m (ε_{av} = 0.00775); and (B) 0.65 m
667 (ε_{av} = 0.0142). Time-averaged seawater velocity vectors in the vertical central plane in flat-
668 panel photobioreactor with a gas-free liquid height of: (C) 1.3 m; and (D) 0.65 m.
669

670

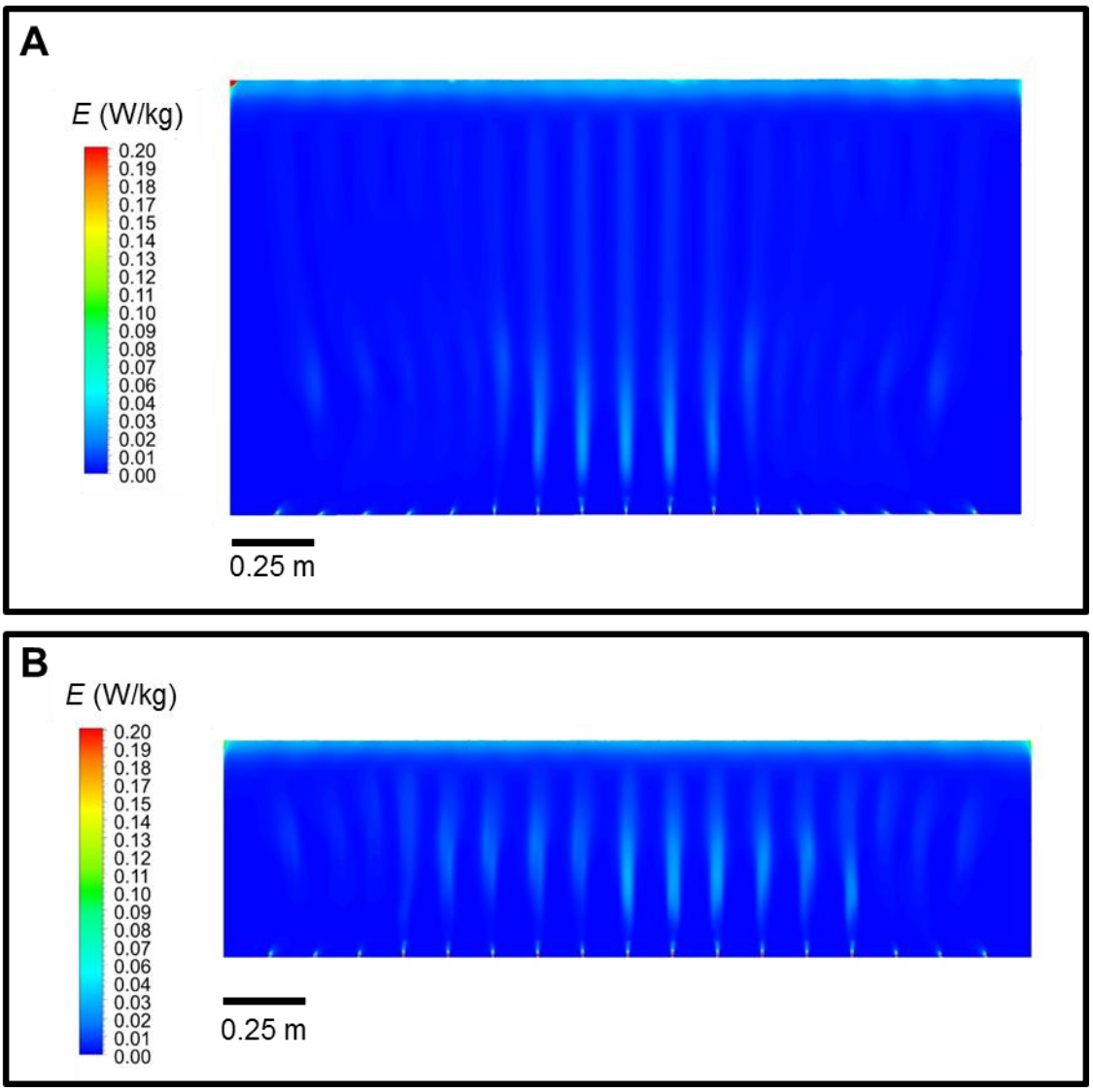

671

672

673 **Fig. 4.** Energy dissipation rate (*E*) values in the liquid phase in the vertical central plane of

674 flat-panel photobioreactor with a gas-free liquid height of: (A) 1.3 m; and (B) 0.65 m.

675

676

677

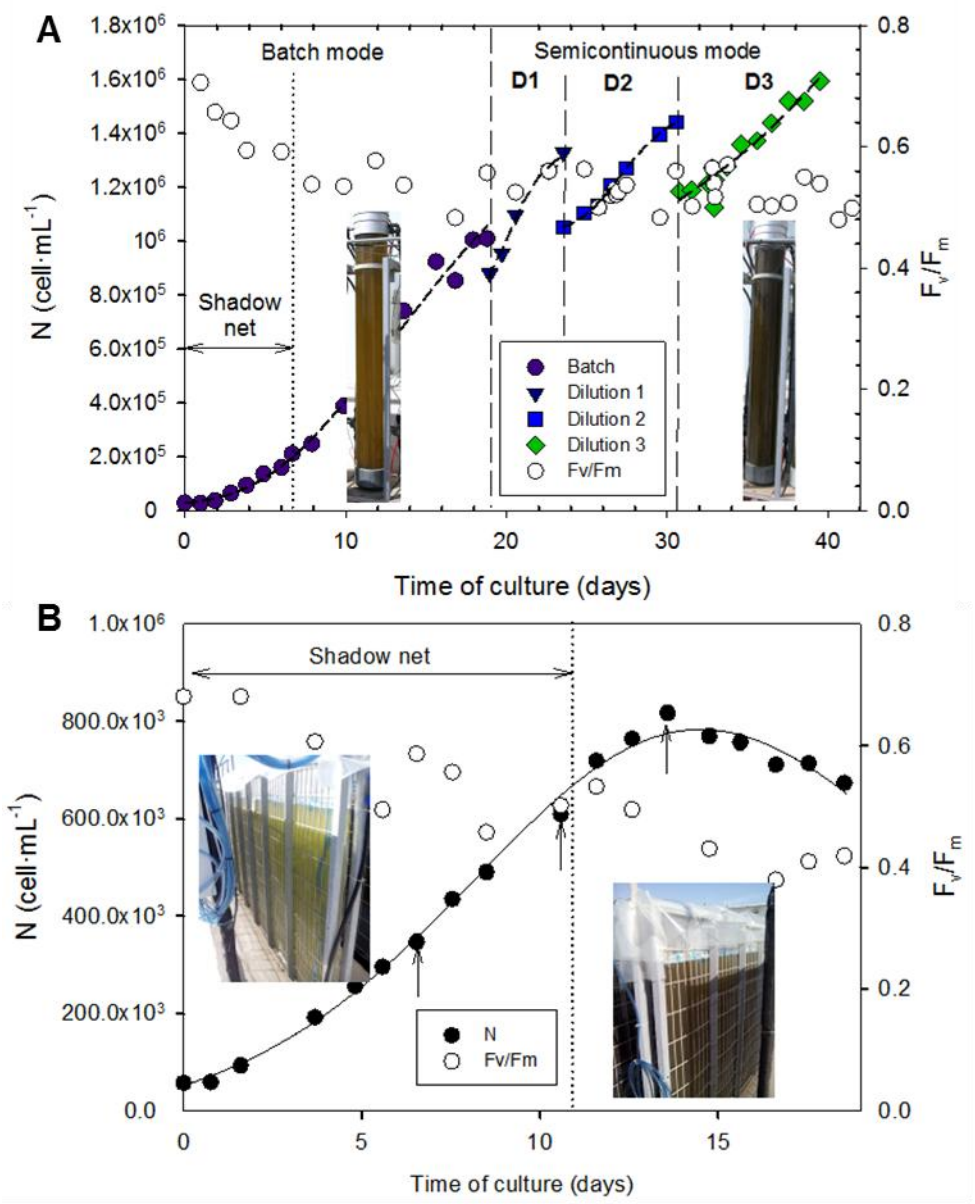

678

679 **Fig. 5.** Variation of cell concentration (*N*) and the F_v/F_m ratio with time during batch and
680 semicontinuous cultures in: (A) bubble column (culture depth = 1.86 m; average dilution rate
681 during semicontinuous culture = 0.04±0.01 day^{-1}); and (B) flat-panel bioreactor (culture depth
682 = 1.3 m; arrows denote the instances of feeding). The inset photographs show the cultures in
683 the different growth phases. Data points are averages for triplicate samples. Standard
684 deviation bars are hidden by the data symbols.

685

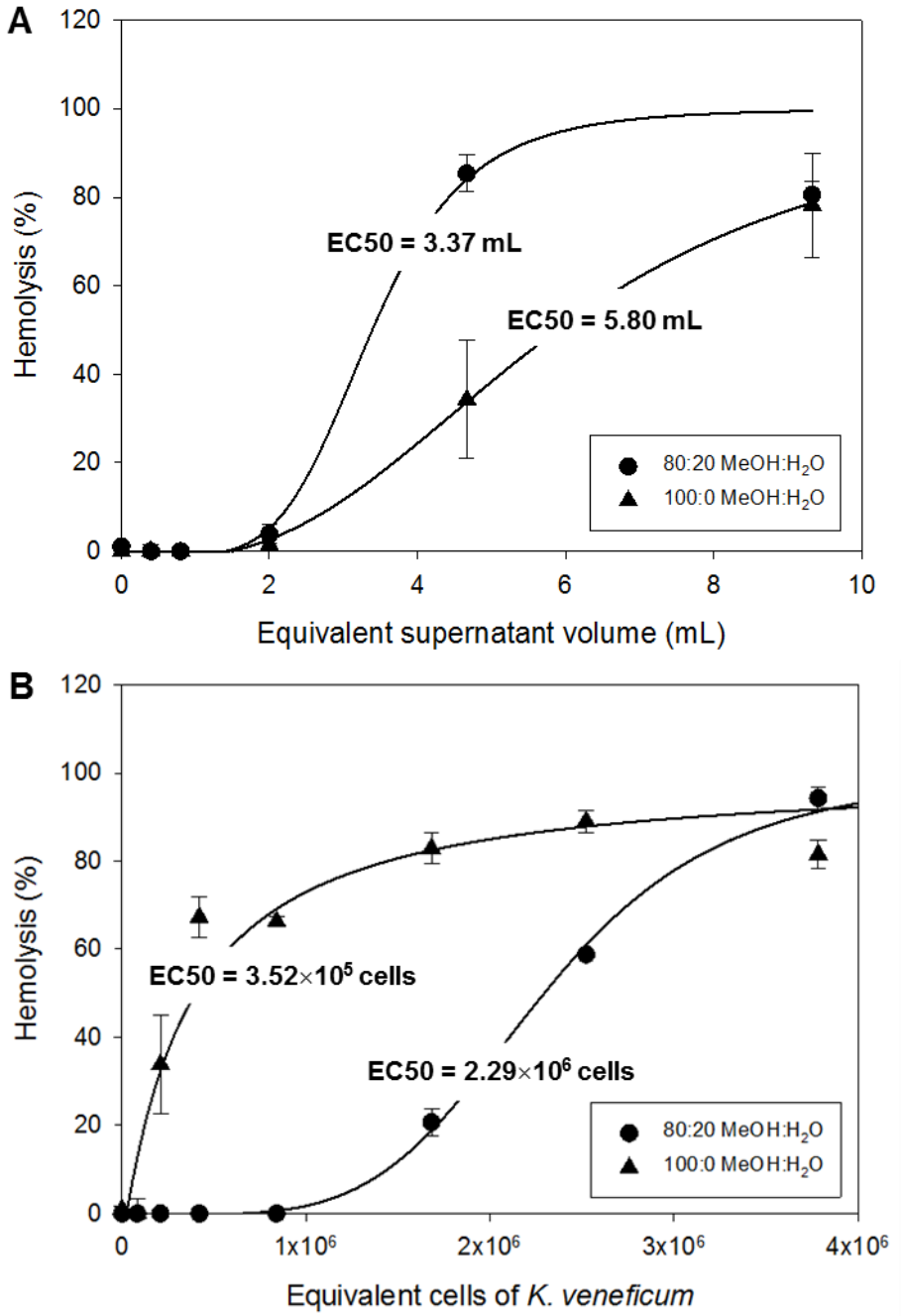

686

687

688 **Fig. 6.** Hemolysis of sheep erythrocytes by extracts of culture supernatant (A) and the cells
689 (B). Data are shown for 80% and 100% methanolic (MeOH) fractions after C18
690 chromatography. Data points are averages for triplicate samples. Standard deviation is shown
691 by vertical bars.